Laboratory soft-x-ray microscope for cryotomography of biological specimens

Michael Bertilson, Olov von Hofsten, Ulrich Vogt, Anders Holmberg, Athanasia E. Christakou, and Hans M. Hertz*

Biomedical and X-Ray Physics, Department of Applied Physics, KTH Royal Institute of Technology/AlbaNova, 10691 Stockholm, Sweden
**Corresponding author: hans.hertz@biox.kth.se*

Received April 15, 2011; accepted May 12, 2011;
posted May 19, 2011 (Doc. ID 145899); published July 14, 2011

Soft-x-ray cryotomography allows quantitative and high-resolution three-dimensional imaging of intact unstained cells. To date, the method relies on synchrotron-radiation sources, which limits accessibility for researchers. Here we present a laboratory water-window microscope for cryotomography. It is based on a $\lambda = 2.48$ nm liquid-jet laser-plasma source, a normal-incidence multilayer condenser, a 30 nm zone-plate objective, and a cryotilt sample holder. We demonstrate high-resolution imaging, as well as quantitative tomographic imaging, of frozen intact cells. The reconstructed tomogram of the intracellular local absorption coefficient shows details down to ~100 nm.

OCIS codes: 180.7460, 110.6955, 180.6900, 170.3880, 340.0340.

Techniques for three-dimensional (3D) and high-resolution imaging of intact cells in their native state are of great interest in cell biology. Moreover, many researchers benefit from having their imaging tools accessible in their home laboratory. Present laboratory-scale high-resolution methods, i.e., superresolution optical [1] and electron cryotomography [2], are valuable tools in biology, but they are essentially limited to thin specimens and thus not applicable to imaging of entire intact cells.

Soft-x-ray microscopy allows several-micron-thick hydrated cells to be imaged at high resolution in a near-native state without chemical fixation, staining or sectioning. Only cryopreservation is needed to avoid radiation damage. The technique utilizes the deep penetration ~10 μm and the natural differential absorption contrast between water and carbon (protein, lipids, etc.) provided by the water-window ($\lambda = 2.3$–4.4 nm, $E =$ 284–540 eV). Diffractive zone-plate objectives are used for imaging and the full-period resolution is currently determined by nanofabrication techniques, rather than the wavelength, to typically 20–100 nm [3]. Since the image contrast depends primarily on absorption, the intracellular structure and its local absorption coefficient (LAC) can be quantified in 3D via computed tomography [4,5]. Synchrotron-based soft-x-ray cryotomography provides 50–70 nm isotropic resolution in 3D of intact cells and currently delivers biologically relevant results [6,7]. Unfortunately, the method has only been available at large high-brightness synchrotron x-ray facilities, which limits its accessibility for a wider community of biologists. The same is valid for the emerging techniques based on lensless hard x-ray coherent diffraction imaging [8].

Laboratory water-window x-ray microscopes based on zone plates and laser-plasma sources [9,10] have, so far, shown imaging with better than 50 nm resolution [11], and tomography on dry dose-resistant objects [12]. Laboratory microscopes with other soft x-ray sources or imaging optics provide less detail [13,14]. All lack the cryogenic capability needed for imaging of hydrated cells.

Here we describe a laboratory soft-x-ray microscope with cryo-microscopy and tomography. We show that it can image intact frozen hydrated cells with an image quality approaching synchrotron quality, and demonstrate its use for quantitative cryotomography.

The microscope operates at $\lambda = 2.48$ nm for maximum transmission in thick specimens, allows tomographic imaging of frozen hydrated biological specimens, and is compact enough to fit on an optical table. Figure 1 shows the arrangement. In brief, it consists of a liquid-jet laser-plasma source, a multilayer condenser mirror, a cryotilt specimen holder, a high-resolution zone-plate objective, and a soft-x-ray sensitive CCD detector.

The soft-x-ray source is produced by focusing high-energy laser pulses (130 mJ/pulse, 100 Hz, 3 ns) from a frequency-doubled ($\lambda = 532$ nm) Nd:YAG laser (Coherent Infinity 40–100) onto the laminar part of a 20-μm-diameter liquid-nitrogen jet [15]. The high focal intensity $\sim 2.5 \cdot 10^{13}$ W/cm^3 produces a 20 μm × 30 μm hot dense plasma with strong, narrow-bandwidth $\Delta\lambda/\lambda < 1/500$ emission lines in the water-window, suitable for imaging with chromatic optics such as zone-plate objectives.

The source is imaged with 1.6× magnification onto the sample with a 58-mm-diameter spherical ($R = 350$ nm) normal-incidence multilayer mirror. It consists of 413 Cr/V bilayers with B_4C interdiffusion barriers. Because of its narrow reflectivity peak, it acts as a monochromator, selecting the ~10^{12} photons/(sr × pulse × line)

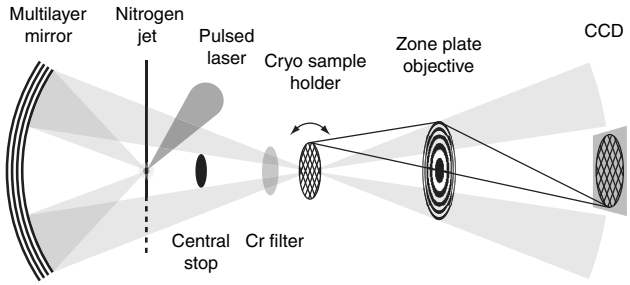

Fig. 1. Microscope arrangement. Soft x rays ($\lambda = 2.48$ nm) from a liquid-jet laser-plasma source illuminate the specimen via a multilayer condenser. The specimen is imaged onto a CCD with a high-resolution zone plate. The cryotilt holder allows tomographic imaging of hydrated biological specimens.

hydrogenlike nitrogen $K\alpha$ line at $\lambda = 2.48$ nm, for which it has an average reflectivity of 0.6%. A 300-nm-thick freestanding chromium filter blocks scattered laser light and separates the source and sample vacuum chambers. Illuminating rays from the condenser heading toward the detector are blocked by a central stop. The resulting hollow-cone illumination has an NA of 0.063 and the illuminated sample area fits well with the $\sim 40\,\mu$m field of view.

The objective is an in-house fabricated [16] nickel zone plate with 99 μm diameter and 30 nm outermost zone width. It is used in the first diffraction order, resulting in a 1.2 mm focal length, 0.041 NA, and a theoretical Rayleigh resolution of 37 nm. The diffraction efficiency of the zone plate is ~9% and it collects ~40% of the illuminating cone due to the 1.5× overmatched condenser aperture. The chromatic aberration caused by its 825 zones expands the diffraction limited depth of focus to $\sim 2\,\mu$m. As a result of the combination of its long focal length with a small source size, the stray-light intensity from nonimaging diffraction orders is low [17]. No stray-light-reducing aperture in the sample plane is therefore needed, which results in less constrained conditions for sample rotation and, thus, facilitates tomographic imaging.

The zone plate images the sample onto a cooled, thinned, back-illuminated 2048×2048 pixel CCD (Princeton Instruments) with $13.5\,\mu\text{m} \times 13.5\,\mu$m pixels and a quantum efficiency of ~0.55%. A magnification of 667 was used throughout the experiments, resulting in 20-nm object-plane pixels. At this magnification, the system typically provides 1000 photons/pixel during a 1 min exposure.

The sample stage is a modified transmission electron microscope (TEM) goniometer stage (FEI), which allows 180° rotation of commercially available TEM sample holders, while the working distance of the zone plate and the current sample holder geometry limit the acquisition angles to ±50°. Liquid-nitrogen-cooled copper shields surround the sample to ensure low water residuals. An optical microscope is positioned above the sample for visual alignment and sample inspection.

We used this laboratory microscope to image yeast cells (*Saccharomyces cerevisiae*) and cells from human immune-system B-cell (721.221/HLA-Cw6) and kidney cell (HEK293T) lines. The human cell lines were cultivated in growth medium and kept in an incubator (37 °C, 5% CO_2) before being harvested according to standard procedure. Yeast cells were simply prepared from dry yeast in a lukewarm dilute sucrose solution. The cells were seeded on carbon-film-coated TEM grids, blotted to remove excess liquid, and quickly plunge-frozen in liquid-nitrogen-cooled liquid ethane. The grids were transferred into the microscope and kept at cryogenic temperatures with a liquid-nitrogen-cooled high-tilt cryotransfer holder (Gatan) during image acquisition.

Figure 2(a) shows a single 60 s exposure of yeast cells in two different states (the denser cells with thicker walls might be yeast spores). Figure 2(b) shows a human B-cell. The image shows enhanced contrast and detail compared to optical microscopy, especially for the dense round features, which most likely are protein-dense granules. The nuclear membrane and nucleoli are also visible. In order to avoid drift-blur, the image was compiled from 6×120 s exposures. In this manner, an image quality

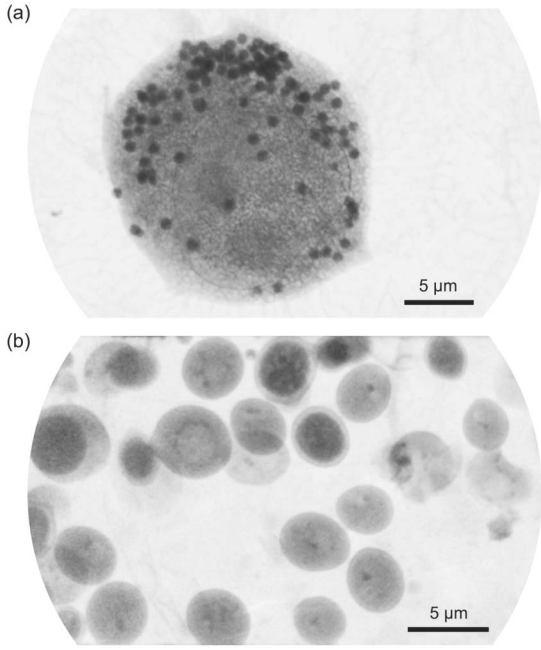

Fig. 2. Frozen hydrated cells imaged in the laboratory x-ray microscope. (a) Yeast cells. (b) Human B-cell. Both images show considerable intracellular structure and detail with natural contrast.

(resolution and contrast) similar to that obtained in single exposures with synchrotron-based microscopes can be obtained, albeit with longer exposure times. Both images in Fig. 2 were flat-field corrected and cropped to show the area of interest.

To demonstrate the tomographic imaging capability of the microscope, a human kidney cell with much structure was selected. It was imaged in a series of 58×120 s exposures, with ~1.5° tilt increments, covering tilt angles between ±44°. A total average dose of <100 MGy was deposited, including the dose from realignment and refocusing. The acquired images I were flat-field corrected, normalized to compensate intensity fluctuations, and aligned using small prominent features as landmarks, and the corresponding projected densities $P = -\ln(I/I_0)$ were calculated from an estimated incident intensity I_0. The local absorption coefficient of the cell was then reconstructed with 40 nm cubic voxels from slightly denoised and resampled projected densities, employing a simultaneous iterative reconstruction technique (SIRT). TomoJ [18] was used for both image alignment and tomographic reconstruction.

Figures 3(a)–3(f) (Media 1) show sections through the tomogram, exhibiting a variety of intracellular features including the nucleus, nucleoli, vacuoles, and more protein-dense unidentified features. The many vacuoles indicate that this particular cell most probably is in the process of necrosis or apoptosis. The smallest visible detail in these sections, estimated from 10% to 90% edge-rise measurements, is ~100 nm. The accuracy in the depth direction is lower due to the missing wedge, but it is sufficient for localizing features in the cell volume. Figure 3(g) (Media 2) shows a surface rendering of prominent cellular features. These features were semimanually segmented according to their LAC and visualized using the Amira software program.

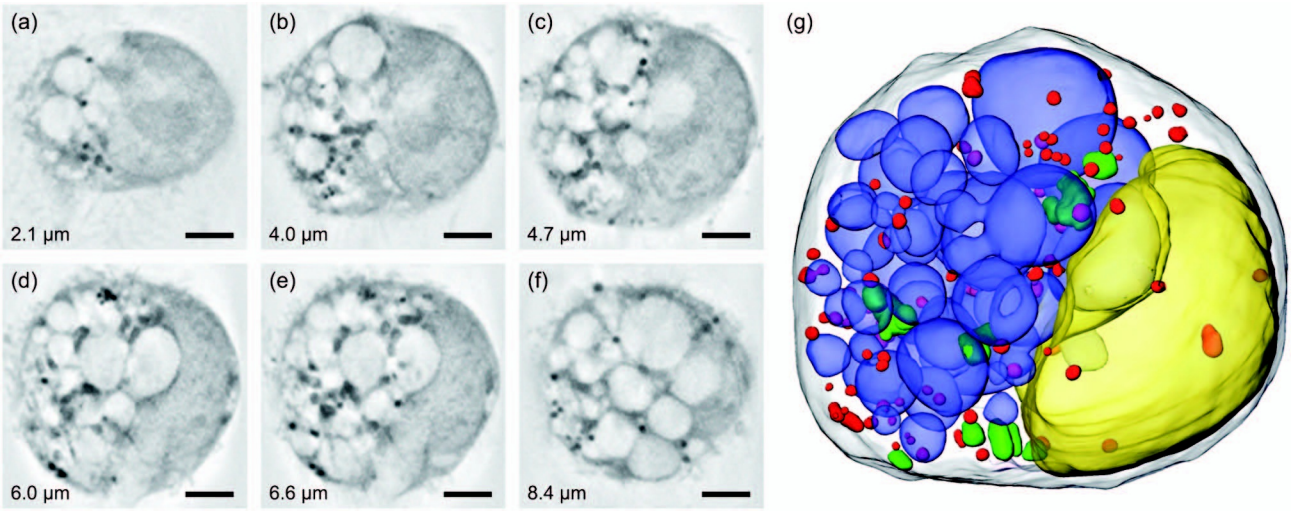

Fig. 3. Laboratory soft x-ray cryotomography of a kidney cell. (a)–(f) Sections through the tomogram at indicated depths (Media 1). Scale bars are 3 μm, and the darker gray corresponds to a higher LAC. (g) Surface rendering of segmented intracellular features (Media 2). Colors indicate nucleus (yellow), vacuoles (blue), and other organelles with higher LAC (green or red).

Note that the achievable tomographic accuracy in this demonstration was limited due to an object size larger than the diffraction-limited depth of focus (DOF), the missing wedge, and noise. Higher accuracy can be obtained for smaller objects or regions of interest by increasing the number of, and signal-to-noise ratio in, the acquired images. Effects of the contrast transfer function and DOF on resolution and quantitative accuracy in soft-x-ray tomography were theoretically investigated in [17].

In summary, we have demonstrated a laboratory soft x-ray microscope for imaging of frozen, hydrated, unstained, intact cells. It provides high-resolution images, as well as quantitative tomograms of the intracellular local absorption coefficient for later segmentation and analysis of the structure. Such imaging of intact cells in a near-native state is of significant importance for studies of the function and structure of biological material. The laboratory scale of this microscope can increase the accessibility of the technique and, thus, its potential scientific impact. Effort is now being put into upgrading the microscope with a 2 kHz laser to reduce exposure times and to reduce the missing wedge. This upgrade will allow tomographic imaging of intact cells with a detail level approaching that of synchrotron microscopes in the local laboratory.

This work was supported by the Swedish Research Council, the Swedish Foundation for Strategic Research, and the Wallenberg Foundation. We thank Magnus Lindblom for zone plates and Hjalmar Brismar for discussions.

References

1. S. W. Hell, Nat. Meth. **6**, 24 (2009).
2. O. Medalia, I. Weber, A. S. Frangakis, D. Nicastro, G. Gerisch, and W. Baumeister, Science **298**, 1209 (2002).
3. A. Sakdinawat and D. Attwood, Nat. Photon. **4**, 840 (2010).
4. D. Weiss, G. Schneider, B. Niemann, P. Guttmann, D. Rudolph, and G. Schmahl, Ultramicroscopy **84**, 185 (2000).
5. C. A. Larabell and M. A. Le Gros, Mol. Biol. Cell **15**, 957 (2003).
6. E. Hanssen, C. Knoechel, N. Klonis, N. Abu-Bakar, S. Deed, M. LeGros, C. Larabell, and L. Tilley, J. Struct. Biol. **173**, 161 (2011).
7. G. Schneider, P. Guttmann, S. Heim, S. Rehbein, F. Mueller, K. Nagashima, J. Heymann, W. Müller, and J. McNally, Nat. Meth. **7**, 985 (2010).
8. H. N. Chapman and K. A. Nugent, Nat. Photon. **4**, 833 (2010).
9. Berglund, Rymell, Peuker, Wilhein, and Hertz, J. Microsc. **197**, 268 (2000).
10. P. A. C. Takman, H. Stollberg, G. A. Johansson, A. Holmberg, M. Lindblom, and H. M. Hertz, J. Microsc. **226**, 175 (2007).
11. O. von Hofsten, M. Bertilson, J. Reinspach, A. Holmberg, H. M. Hertz, and U. Vogt, Opt. Lett. **34**, 2631 (2009).
12. M. Bertilson, O. von Hofsten, U. Vogt, A. Holmberg, and H. M. Hertz, Opt. Express **17**, 11057 (2009).
13. M. Benk, K. Bergmann, D. Schäfer, and T. Wilhein, Opt. Lett. **33**, 2359 (2008).
14. M. Hoshino and S. Aoki, Appl. Phys. Express **1**, 067005 (2008).
15. P. A. C. Jansson, U. Vogt, and H. M. Hertz, Rev. Sci. Instrum. **76**, 043503 (2005).
16. J. Reinspach, M. Lindblom, O. V. Hofsten, M. Bertilson, H. M. Hertz, and A. Holmberg, Microelectron. Eng. **87**, 1583 (2010).
17. M. Bertilson, O. von Hofsten, H. M. Hertz, and U. Vogt, Opt. Express **19**, 11578 (2011).
18. C. Messaoudi, T. Boudier, C. Sorzano, and S. Marco, BMC Bioinf. **8**, 288 (2007).